Inorganic Chemistry

ARTICLE

pubs.acs.org/IC

Templated Construction of a Zn-Selective Protein Dimerization Motif

Eric N. Salgado, Jeffrey D. Brodin, Magnus M. To, and F. Akif Tezcan*

Department of Chemistry and Biochemistry, University of California, San Diego, 9500 Gilman Drive, MC 0356, La Jolla, California 92093, United States

Supporting Information

ABSTRACT: Here, we report that the approach of metal-templated ligand synthesis can be applied to construct a dimeric protein assembly (^{BMOE}RIDC1$_2$), which is stabilized by noncovalent interactions and flexible covalent cross-linkers around the Zn templates. Despite its flexibility, ^{BMOE}RIDC1$_2$ selectively binds Zn^{II} over other divalent metals and undergoes dimerization upon metal binding. Such simultaneous fulfillment of plasticity and selectivity is a hallmark of cellular signaling events that involve ligand/metal-induced protein dimerization.

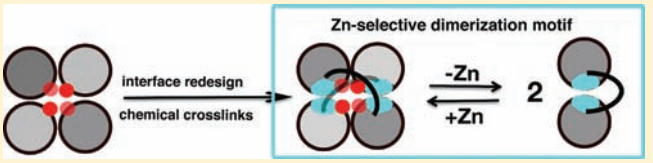

INTRODUCTION

We describe the metal-templated construction of a protein complex that undergoes dimerization in selective response to Zn binding. In previous examples of designed molecular recognition, chemists have devised small organic building blocks that self-assemble into discrete supramolecular structures upon selective binding of organic or inorganic substrates.[1] Such systems include Rebek and Ajami's[2] and Gibb and Gibb's[3] cavitands that dimerize into nanocapsules via hydrocarbon sequestration and Lehn et al.'s[4] and Raymond and Caulder's[5] helicates that selectively self-organize into higher-order assemblies upon metal complexation. Our work represents an extension of such synthetic work into the realm of protein building blocks while simultaneously demonstrating that a traditional approach in coordination chemistry (metal-templated ligand synthesis) can readily lead to the emergence of a selective, chemically induced protein dimerization event, which is a cornerstone of cellular signaling pathways.[6]

Proteins are nature's premier ligand scaffolds for constructing functional metal centers, as they can afford an exquisite tuning of metal selectivity and reactivity through a combination of covalent and noncovalent interactions. An absolute requirement for the generation of any metallic (or nonmetallic) active site with a specialized function is that it is *internalized* within a network of such interactions.[7] We have proposed that a straightforward route for engineering functional metal sites may proceed through a metal-mediated nucleation of multiprotein complexes and a subsequent stabilization of the resulting protein interfaces around the now-internalized metal centers.[8,9] This approach was termed metal-templated interface redesign (MeTIR). The possibility of an evolutionary pathway similar to MeTIR has previously been suggested by Bolin et al.[10] and Armstrong[11] for the vicinal oxygen chelate (VOC) superfamily of metalloenzymes and by Hol and Volbeda[12] for hemocyanin and other dioxygen binding proteins. In further support, the inspection of many sophisticated metal active sites or binding pockets for nonmetallic substrates reveals that they are formed in the interfaces between protein domains or subunits,[13,14] which likely were independently folded units.[15]

A synthetic analogy for MeTIR is provided by the time-proven method of metal-templated ligand synthesis, first reported by Busch and Thompson[16] and adopted by others,[17−19] in which a macrocyclic chelate is first organized and then covalently assembled around a metal ion. Inspired by this approach, we recently reported that a Zn^{II}-mediated, D_2-symmetrical, tetrameric superstructure of a monomeric protein, cytochrome cb_{562} (Zn$_4$:MBPC1$_4$, Figure 1a and b), can be converted into a stable, unimolecular assembly (^{C96}RIDC1$_4$, Figure 1c) through the installment of stable covalent and noncovalent bonds into the interfaces surrounding the four Zn centers.[20] ^{C96}RIDC1$_4$ is not only one of the most stable multiprotein complexes ever engineered but also displays impressive Zn^{II} selectivity over other divalent ions, including Cu^{II}, and couples Zn^{II} binding to a large conformational change akin to a metal-dependent signaling protein.[20] The seemingly contradictory traits of stability—both in terms of oligomerization and metal binding—and flexibility are afforded by the combination of fluid hydrophobic interactions incorporated into one set of interfaces (interface 1, *i*1) and short disulfide linkages (Cys96−Cys96′) built into a second set (*i*2) (Figure 1c). In this study, we envisioned that the lengthening of the interfacial covalent linkages may further increase the flexibility of the assembly and result in the formation of alternative oligomeric forms while still retaining metal selectivity, which is the most basic but essential metal-based function. We report that such long covalent linkages across *i*3 result in the formation of a stable, folded structure consisting of two protomers (^{BMOE}RIDC1$_2$) that dimerizes into a tetrameric form (Zn$_4$:^{BMOE}RIDC1$_4$) upon selective Zn binding (Figure 1d).

Received: April 11, 2011
Published: June 07, 2011

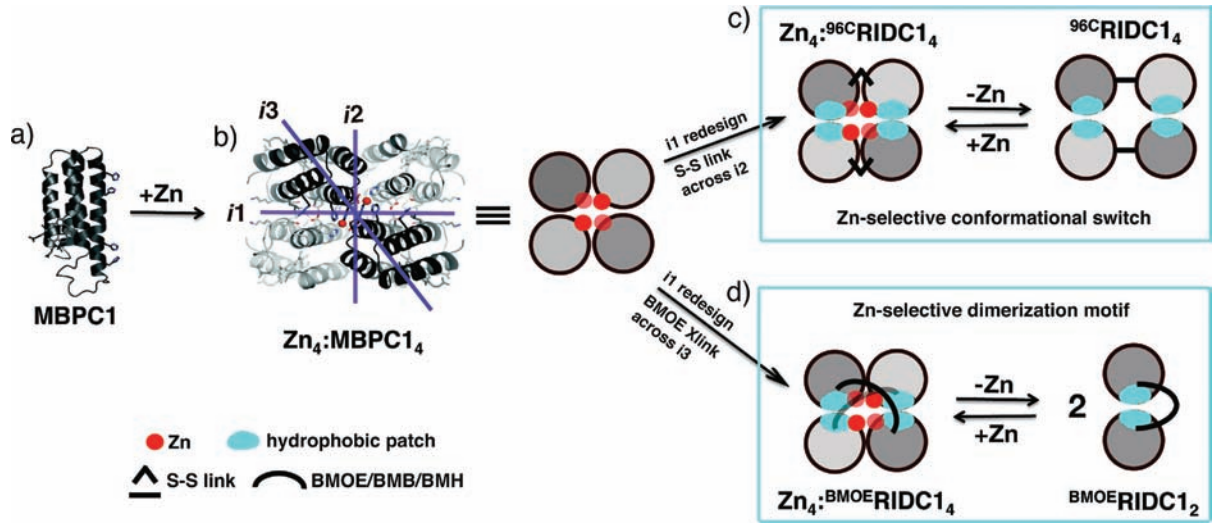

Figure 1. Templated construction of Zn-selective protein complexes. The metal-chelating variant of cyt cb_{562}, MPBC-1 (a), undergoes Zn-mediated tetramerization into the D_2-symmetrical Zn_4:$MBPC1_4$ (b). (c) The combination of fluid, hydrophobic interactions installed into the *i*1 interface with a disulfide bond across *i*2 produces a tetramer, $^{96C}MBPC1_4$, that undergoes a Zn-selective conformational change,[20] whereas the combination of *i*1 interactions with a flexible linker across *i*3 (d) yields a Zn-selective dimerization motif (this study).

RESULTS AND DISCUSSION

The three C_2-symmetric interfaces of Zn_4:$MBPC1_4$ are highlighted in Figure 1b and shown in detail in Figure S1, Supporting Information. Of these, *i*1 is the most extensive and closely packed and readily lent itself to stabilization through the insertion of computationally prescribed and mostly hydrophilic-to-hydrophobic mutations (R34A/L38A/Q41W/K42S/D66W/V69I, blue patches in Figure 1) to generate RIDC1.[8] As the dihedral symmetry of the Zn-driven tetramer dictates, the combination of the stabilizing, noncovalent interactions in *i*1 with a short disulfide bond across the *i*2 interface (via the T96C mutation) should result in the formation of a stable tetramer ($^{C96}RIDC1_4$), as was borne out through hydrodynamic and crystallographic investigations.[20] *i*3, in contrast, is a minimal interface (490 Å^2 buried surface) formed entirely by the inner Zn coordination sphere (Figure S1) and is not amenable to redesign or cross-linking through a disulfide bond. We surmised that a long, flexible chemical linker incorporated across *i*3 into RIDC1 could result in the formation of either a folded-over dimer (stabilized by the hydrophobic mutations in *i*1; Figure 1d) or a D_2-symmetrical tetramer in the absence of Zn, in effect mimicking what nature accomplishes through genetically encoded peptide linkers for fusing proteins in order to realize the "chelate effect".[11,21] Toward this end, we replaced the symmetrically related pairs of Gly82 residues (Figure S1) near the vertex of *i*3 with cysteines for chemical coupling through bis-maleimide functionalized cross-linkers.

The cross-linkers used (Figure 2), bis-maleimidoethane (BMOE), bis-maleimidobutane (BMB), and bis-maleimidohexane (BMH), have spacer arm lengths of 8.0 Å, 10.9 Å, and 13.0 Å, respectively, and are all expected to readily cover the anticipated $^{C82}S—^{C82'}S$ distance of 10−11 Å. The coupling reactions proceed cleanly, whereby the cross-linking agents are added slowly to the protein solution to promote the formation of cross-coupled dimers over singly modified (saturated) monomers. The dimers, $^{BMOE}RIDC1_2$, $^{BMB}RIDC1_2$, and $^{BMH}RIDC1_2$, were separated from monomers through size-exclusion chromatography, and their compositions were confirmed by mass spectroscopy (12 349 Da for the parent ^{82C}RIDC1; 24 918 Da, 24 946 Da, and 24 974 Da for the BMOE, BMB, and BMH cross-linked dimers, respectively).

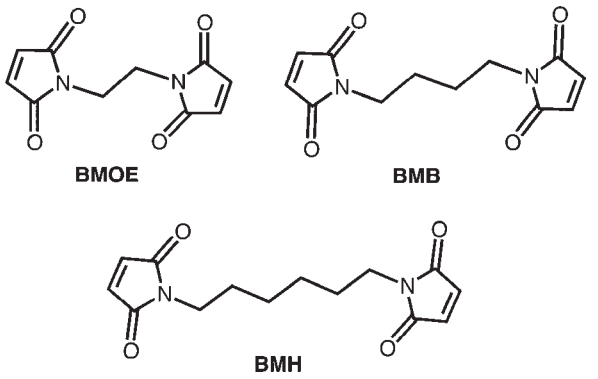

Figure 2. Cys-specific, bis-maleimide functionalized cross-linkers.

We first probed whether the cross-linked dimers assemble into the same Zn-mediated D_2-symmetric tetrameric architecture that formed the basis of templated redesign. Sedimentation velocity (SV) experiments show that even at a concentration of 2.5 μM (lowest dimeric concentration measurable), $^{BMOE}RIDC1_2$, $^{BMB}RIDC1_2$, and $^{BMH}RIDC1_2$ all are entirely tetrameric in the presence of Zn^{II}, with a peak sedimentation coefficient of approximately 4.5 S (Figure 3), which matches that of the parent complex, Zn_4:$RIDC1_4$.[8] In comparison, the non-cross-linked RIDC-1 shows a distribution of 60% dimer and 40% tetramer under comparable solution conditions (5 μM RIDC1 and Zn^{II}). Although SV is a nonequilibrium technique, this comparison nevertheless indicates the stabilization of Zn-induced tetramers due to cross-linking, likely due to entropic reasons. The crystal structures of the Zn adducts of $^{BMOE}RIDC1_2$ (PDB ID: 3QVY), $^{BMB}RIDC1_2$ (PDB ID: 3QW0), and $^{BMH}RIDC1_2$ (PDB ID: 3QW1) were determined at 2.3 Å, 1.8 Å, and 2.6 Å resolution, respectively. As shown in a structural superposition in Figure 4a, the supramolecular architectures of the resulting complexes are identical to one another, and to Zn_4:$MBPC1_4$[22] and Zn_4:$RIDC1_4$.[8]

dx.doi.org/10.1021/ic200746m |*Inorg. Chem.* 2011, 50, 6323–6329

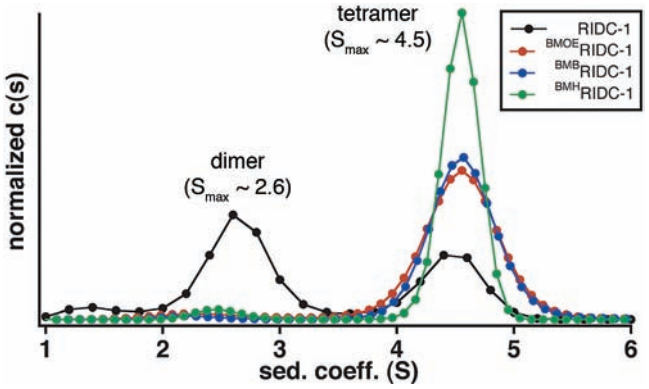

Figure 3. Hydrodynamic analysis of maleimide cross-linked constructs in the presence of Zn^{II}. Sedimentation velocity (SV) profiles for various cross-linked (2.5 μM dimer) and a non-cross-linked construct (5 μM monomer) in the presence of 5 μM Zn^{II} demonstrate almost full conversion to a Zn^{II} induced tetramer of the three cross-linked constructs at relatively low protein and metal concentrations.

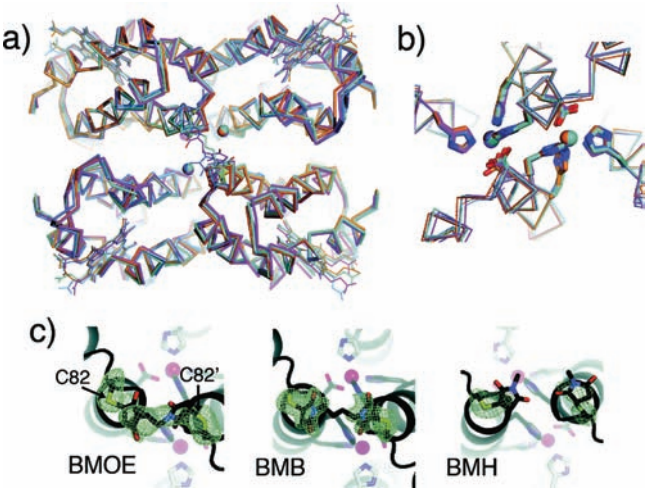

Figure 4. Comparison of the supramolecular structures of the Zn^{II} mediated tetramers of maleimide cross-linked constructs. (a) Structural superposition of Zn_4:RIDC1$_4$ (orange), Zn_4:^{BMOE}RIDC1$_4$ (magenta), Zn_4:^{BMB}RIDC1$_4$ (cyan), and Zn_4:^{BMH}RIDC1$_4$ (marine). (b) Superposition of the Zn coordination environments (same coloring scheme). (c) F_o-F_c omit electron difference density maps (2.5 σ) of the BMOE, BMB, and BMH cross-linkers. For BMH, the hexane linker region was not modeled due to the lack of electron density.

Importantly, the Zn-coordination environments, which lie in close proximity to the cross-linking sites, are unchanged as intended by the use of flexible linkers (Figure 4b). The electron density for the entire length of the BMOE linker is evident, while for the longer BMB and BMH linkers only the Cys82−thioether−succinamide moiety can be discerned (Figure 4c).

Having verified their Zn-driven assembly into the desired "macrocyclic" architecture, we next investigated the structures of ^{BMOE}RIDC1$_2$, ^{BMB}RIDC1$_2$, and ^{BMH}RIDC1$_2$ in the absence of Zn. SV measurements indicate that dimers are the predominant oligomeric form under the conditions tested for all cross-linkers. At low protein concentrations (2.5 μM), a small population of possibly tetrameric species (4.5−4.8 S) is observed (Figure 5a), while at higher concentrations (>25 μM), the SV distributions for such high-order aggregates become considerably broader and tail into larger sedimentation coefficients that are suggestive of linear polymeric chains (Figure, 5b). These results suggest that the cross-linked dimers prefer to adopt the folded-over conformation rather than a preorganized tetramer reminiscent of the Zn-induced structure.

Despite extensive efforts, we could not crystallize the cross-linked dimers in the absence of metal ions, which likely is a result of their flexibility as well as their tendency to form large aggregates at high concentrations. In order to gain some insight into the structures of the cross-linked dimers, we compared their experimentally determined sedimentation coefficients—which are dependent on not only molecular weight but also shape—to those of various theoretical dimeric conformations of ^{BMOE}RIDC1$_2$ (Figure 5c) using Hydropro.[23] These simulations show that as the BMOE dimer transitions from a fully extended configuration to a compact form, its sedimentation coefficient increases from 2.2 to 2.6 S, which is the lower end of the observed range (2.6−2.8 S) for the cross-linked dimers. Validating this analysis, the maximal sedimentation coefficient of the structurally characterized, antiparallel dimer RIDC1$_2$ was determined to be ~2.75 S,[8] which is the most compact structure shown in the series (Figure 5c). On the basis of these findings, we conclude that the chemically cross-linked dimers likely assume a folded structure in solution, driven by the interactions between hydrophobic residues installed for *i*1 redesign.

Given that the cross-linked dimers in their folded form should have many metal-coordinating residues (His, Glu, and Asp) in close proximity and should be relatively flexible, one would expect them to promiscuously coordinate different transition metal ions. Indeed, Co^{II}, Ni^{II}, or Cu^{II} binding to ^{BMOE}RIDC1$_2$ all induce the formation of a tetrameric species, with a maximal sedimentation coefficient of 4.5 identical to that of Zn_4:^{BMOE}RIDC1$_4$ (Figure 6a). However, since the redesign of *i*1 and the placement of cross-linkers across *i*3 were based on the four tetrahedral Zn templates, we anticipated that there should be increased affinity for Zn^{II} binding relative to the other divalent metal ions. To test this possibility, metal binding competition assays were performed with the metal chelating fluorophore, MagFura-2,[24] whereby increasing concentrations of Co^{II}, Ni^{II}, Cu^{II}, or Zn^{II} were titrated into a mixture of ^{BMOE}RIDC1$_2$ and MagFura-2, and the changes in MagFura-2 fluorescence were monitored (Figure 6b−d and Figure S2, Supporting Information). In parallel, titrations were performed to determine the affinity of Mag-Fura-2 for these metal ions (Figure S3, Supporting Information), which yielded similar values to those previously reported.[25,26] Because ^{BMOE}RIDC1$_2$ does not self-associate into a preformed tetramer in the absence of metal binding, and the titration solutions contain a mixture of ^{BMOE}RIDC1$_2$ and ^{BMOE}RIDC1$_4$ in their various metal-bound forms, it is not possible to extract accurate metal binding equilibrium constants. Nevertheless, the titrations show that ^{BMOE}RIDC1$_4$ can accommodate four equivalents each of Co^{II}, Ni^{II}, or Zn^{II} with affinities that rival that of MagFura-2 for those ions. The competition isotherms can be reasonably well described by a 4-equivalent-binding-site model, yielding half-saturation concentrations of 9 μM for Co^{II}, 0.5 μM for Ni^{II}, and 0.04 μM for Zn^{II} (Table 1). It should be noted that these are not true dissociation constants, but rather approximate metal concentrations where half of the starting ^{BMOE}RIDC1$_2$ population is converted into the fully metal-bound M_4:^{BMOE}RIDC1$_4$ species. Given that *i*, *i*+4 bis-histidine motifs on α-helices—which constitute the metal

dx.doi.org/10.1021/ic200746m |*Inorg. Chem.* 2011, 50, 6323–6329

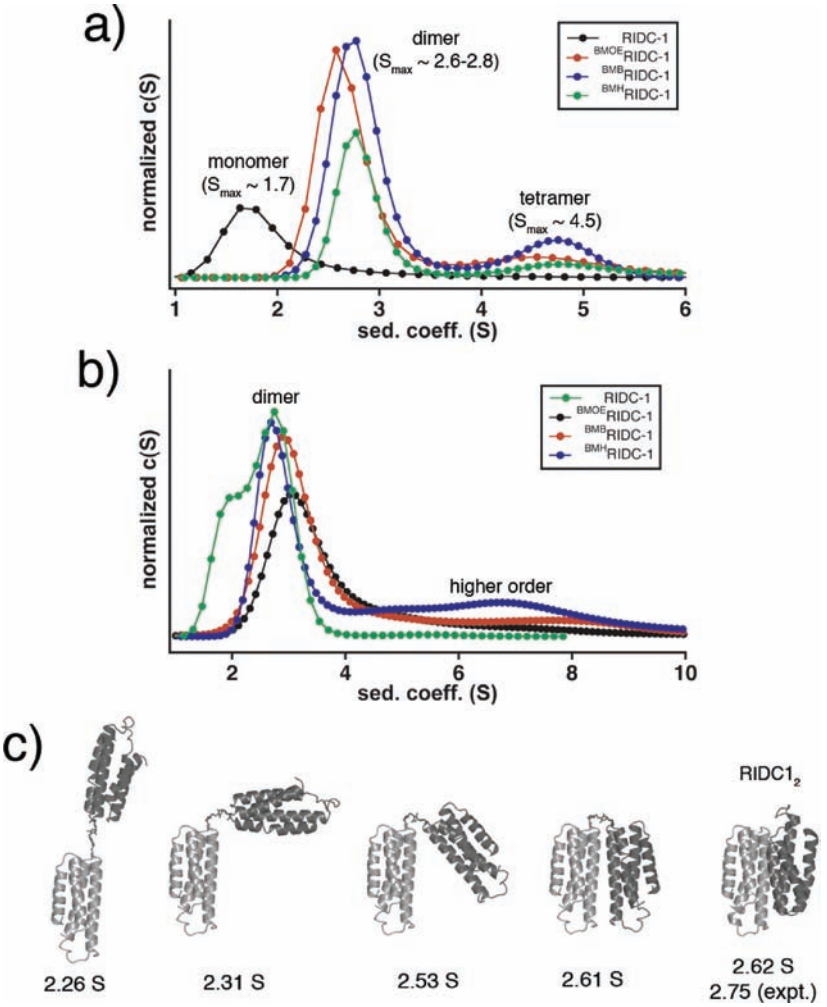

Figure 5. Hydrodynamic analysis of metal-free maleimide cross-linked constructs. (a) Sedimentation velocity (SV) profiles for various cross-linked (2.5 μM dimer) and a non-cross-linked construct (5 μM monomer) in the absence of metals. (b) Same as in part a, but at 25 μM and 50 μM concentrations, respectively, highlighting the presence of higher-ordered species formed by the cross-linked constructs even in the absence of any metal ions. (c) Hypothetical conformations for $^{BMOE}RIDC1_2$ and their calculated sedimentation coefficients. The right-most structure is that of crystallographically characterized $RIDC1_2$ (noncross-linked) with its calculated and experimentally determined sedimentation coefficient.

binding motifs on the parent MBPC1 molecule—bind Co^{II}, Ni^{II}, or Zn^{II} with micromolar affinities that are within an order of magnitude of each other ($K_{d\text{-}Zn} \approx K_{d\text{-}Ni} < K_{d\text{-}Co}$),[27,28] our results clearly show increased thermodynamic selectivity for Zn^{II} coordination over the other two ions.

The ultimate test for Zn^{II} selectivity is provided by Cu^{II}, which lies atop the Irving—Williams series[29] for the relative stabilities of divalent metal complexes ($Mn^{II} < Fe^{II} < Co^{II} < Ni^{II} < Cu^{II} > Zn^{II}$), and readily outcompetes Zn^{II} for most natural and synthetic Zn-specific binding sites.[30−32] This is particularly the case for flexible peptides or proteins that cannot impose steric constraints to offer selectivity between metal ions.[33] In accord with the high affinity of Cu^{II} for protein-based donor atoms, our titrations show that $^{BMOE}RIDC1_4$ has at least 12 binding sites for Cu^{II} that can compete with MagFura-2 (i.e., their K_d's are within an order of magnitude of 8.5 nM;[34] Figure 6e), some likely on the surface and some in the core. The high plurality of Cu^{II} binding to $^{BMOE}RIDC1_4$ and the availability of surface binding sites make it challenging to assess the Zn^{II} versus Cu^{II} selectivity of the internal coordination sites through titrations. We therefore cocrystallized $^{BMOE}RIDC1_2$ in the presence of a mixture of Zn^{II} and Cu^{II}. The structure of the resulting complex (PDB ID: 3QVZ) was determined at 2.6 Å resolution, which revealed that it possesses the same supramolecular architecture as Zn_4:$^{BMOE}RIDC1_4$, with four metals associated with the core and seven with the surface of the tetramer (Figure 7). To identify these metal ions, anomalous difference maps were calculated using X-ray diffraction data collected at the Zn and Cu K-edges (1.265 and 1.377 Å). These maps indicate the core ions to be Zn, which display anomalous scattering only at the Zn K-edge and not at the Cu K-edge, and the majority (6 out of 7) of surface ions to be Cu. X-ray fluorescence scans further confirm the presence of both Cu and Zn in the thoroughly washed crystals (Figure S4, Supporting Information).

Subsequently, we investigated through size exclusion chromatography (SEC) whether Zn_4:$^{BMOE}RIDC1_4$ is a true thermodynamic product. The SEC elution profile of Zn_4:$^{BMOE}RIDC1_4$ run in the presence of Zn indicates the presence of both the tetrameric and the dimeric (as well as higher-order) species (Figure S5, Supporting Information).[35] Although the observed dimeric species is a minor component, as would be predicted from the SV experiments (Figure 3a), the SEC findings suggest

dx.doi.org/10.1021/ic200746m |*Inorg. Chem.* 2011, 50, 6323–6329

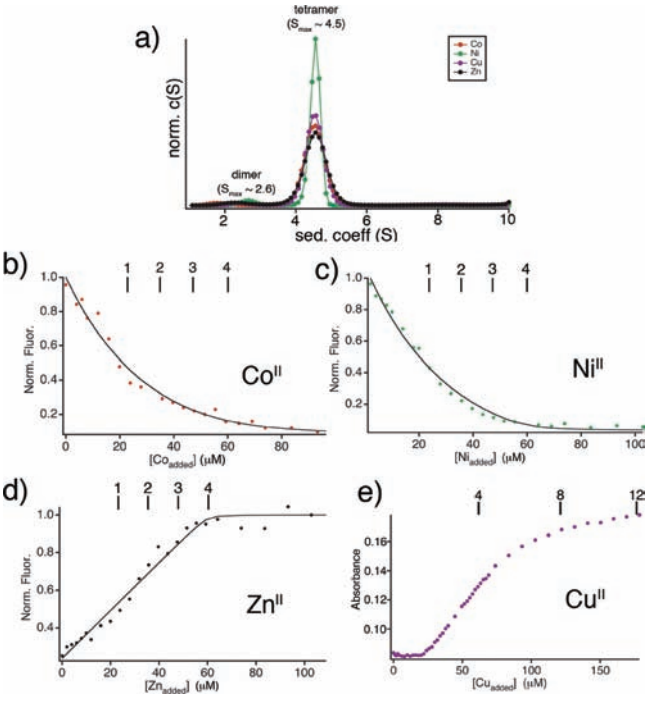

Figure 6. ^{BMOE}RIDC1$_2$ tetramerization mediated by various divalent metal ions with a preference for Zn^{II} binding. (a) SV profiles for the 2.5 μM ^{BMOE}RIDC1$_2$ dimer in the presence of 5 μM Co^{II}, Ni^{II}, Cu^{II}, and Zn^{II}, reflecting the formation of a tetrameric species on binding all four metal ions. (b–d) Binding isotherms for Mag-Fura-2:^{BMOE}RIDC1$_2$ competition experiments with (b) Co^{2+}, (c) Ni^{2+}, and (d) Zn^{2+}, with tick marks shown on the top x axis that correspond to theoretical titration end points for the indicated number of binding sites per tetramer. Solid lines represent fits obtained using DynaFit to a 4-equivalent-binding-sites model, with K_d values listed in Table 1. Cu^{2+} competition experiments (e) demonstrate 12 metal binding events.

Table 1. Apparent Dissociation Constants for Divalent Metal Ion Adducts of Mag-Fura2 and ^{BMOE}RIDC1$_2$

	K_d (μM)	
metal	Mag-Fura-2	^{BMOE}RIDCl$_2$
Zn	0.047 (0.005)	0.041 (0.010)
Ni	0.175(0.014)	0.54 (0.055)
Co	1.41 (0.22)	9.29(1.02)

that Zn$_4$:^{BMOE}RIDC1$_4$ is in exchange with its dimeric form in solution, and that Zn versus Cu selectivity observed under crystallization conditions likely is thermodynamically driven.[36] We attribute the thermodynamic basis for Zn selectivity not only to the formation of a covalently and noncovalently stabilized macrocycle built around the tetrahedral Zn coordination sites but also to the fact that this macrocyle has been programmed to house four Zn ions in its interior, all of which contribute to the overall stability of Zn$_4$:^{BMOE}RIDC1$_4$ formation.

In summary, we have shown here that a traditional approach in synthetic coordination chemistry (metal-templated ligand synthesis) can be applied to the design of a large and dynamic protein assembly, which displays an extent of Zn selectivity that is challenging to achieve in small molecule systems. The advantage of proteins as ligand scaffolds lies in their chemically rich surfaces that enable the formation of an extensive network of stable, yet reversible noncovalent interactions around the metal centers. The ensuing, simultaneous fulfillment of plasticity and selectivity, such as that displayed in our system, is a hallmark of all cellular signaling systems, and particularly those that couple selective metal binding to conformational changes or oligomerization to activate downstream processes, such as the prototypical EF-hand signaling proteins (calmodulin,[37] S100[38]) or any metalloregulatory gene transcription factor.[39]

EXPERIMENTAL SECTION

Protein Mutagenesis. Purification, Modification with Cross-linkers. The G82C-RIDC1 cyt cb_{562} construct (^{C82}RIDC1) was generated, expressed, and purified according to published procedures.[22,40,41] Purified ^{C82}RIDC1 was buffer-exchanged into 20 mM TRIS (pH 7) and 50 mM dithiothreitol (DTT) and concentrated using Amicon stirred cells with MW = 10 kDa cutoff filters. Concentrated protein was eluted through a 10 DG desalting column (BioRad) to eliminate excess DTT and diluted with an appropriate volume of 20 mM TRIS (pH 7) to yield a protein concentration of 100 μM. Concentrated stock solutions of BMOE, BMB, or BMH (Pierce) were added to the sample in 10 equal aliquots every 30 s over 5 min to give a final cross-linker concentration of 100 μM. The reaction was then allowed to proceed at room temperature under constant stirring for 30 min. Cross-linking reactions were quenched by the addition of 50 mM DTT and allowed to incubate at room temperature for 15 min. Cross-linking yields were approximately 50%. Cross-linked proteins were subsequently purified through multiple size exclusion chromatography runs using a Pall ACA54 resin (fractionation range = 5–70 kDa) using an elution buffer of 20 mM TRIS (pH 7) and 150 mM NaCl. Dimer purity was assessed by SDS-PAGE electrophoresis, and the compositions of the dimers were verified by MALDI mass spectrometry.

Analytical Ultracentrifugation and SV Simulations. Sedimentation velocity (SV) measurements were made on a Beckman XL-I Analytical Ultracentrifuge (Beckman-Coulter Instruments) using an An-60 Ti rotor at 41 000 rpm for a total of 250 scans per sample. Data were collected at 415 nm for low concentration (2.5 μM cross-linked dimer, 5 μM RIDC1 monomer) samples and 560 nm for higher concentrations (25 μM cross-linked dimer). All data were processed in SEDFIT[42] with the following fixed parameters: buffer density (r) = 0.99764 g/mL; buffer viscosity = 0.0089485 poise; Vbar, which was calculated to be 0.7310 mL/g for ^{BMOE}RIDC1$_2$ and ^{BMB}RIDC1$_2$ and 0.7306 mL/g for ^{BMH}RIDC1$_2$. The buffer density (ρ) and viscosity for 20 mM TRIS (pH 7) were calculated through SEDNTERP (http://www.jphilo.mailway.com/default.htm). Theoretical sedimentation coefficients were calculated using Hydropro version 7.C,[23] using the same parameters employed in SV data processing.

Crystallography. Crystals of all cross-linked dimers were obtained by sitting drop vapor diffusion at room temperature. The crystallization conditions for the four different crystal forms described in this study are listed in Tables S1 and S2 (Supporting Information), along with corresponding data collection and refinement statistics. All protein stock solutions were in a 20 mM TRIS (pH 7) buffer. Appropriate crystals were transferred to a solution of mother liquor containing 20% glycerol as a cryoprotectant and frozen in liquid nitrogen prior to data collection at 100 K.

Data were integrated using MOSFLM and scaled in SCALA,[43] except for Zn$_4$:^{BMB}RIDC1$_4$, which was processed using SAINT and Bruker SADABS. All structures were determined through molecular replacement with MOLREP,[44] using the RIDC1 monomer structure (PDB ID: 3HNI) as the search model, followed by rigid-body, positional, thermal, and TLS refinement with REFMAC[45] using appropriate noncrystallographic symmetry restraints. The crystals for both forms of

dx.doi.org/10.1021/ic200746m |Inorg. Chem. 2011, 50, 6323–6329

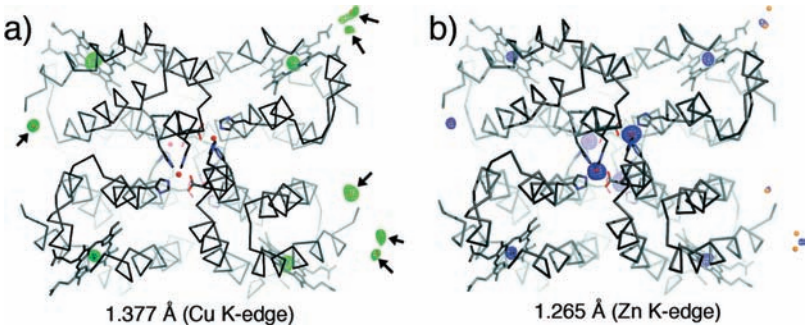

Figure 7. Structure of Zn_4:^{BMOE}RIDC1$_4$ grown in the presence of Cu^{II}. A ribbon representation of Zn_4:^{BMOE}RIDC1$_4$ crystallized in the presence of $CuSO_4$ is shown along with the anomalous difference maps generated from data collected (a) at the Cu K-edge (green, 5 σ) and (b) at the Zn K-edge (blue, 5 σ). The surface-associated Cu ions are shown with arrows in part a. The heme Fe centers as well as well-ordered surface Cu ions have anomalous contributions at both energies, whereas the core Zn ions only contribute at the higher energy Zn K-edge.

Zn_4: ^{BMOE}RIDC1$_4$ (crystallized in the presence and the absence of $CuSO_4$) were found to have 48% and 44% twin fractions, respectively. Both data sets were refined using intensity-based twin refinement as implemented in REFMAC using the twin operator: −1.000 h−1.000k, 1.000k, −l. All structures were manually built in COOT[46] to produce the final models. All figures were produced using PYMOL.[47]

Metal Binding Titrations. For Mag-Fura-2 competition titrations, 1 mg of Mag-Fura-2 (Invitrogen) was resuspended in 1 mL of Millipore purified water. The Mag-Fura-2 concentration was determined using an extinction coefficient of 22 000 M^{-1} cm^{-1} at 369 nm. The titrations for determining Mag-Fura-2 affinities for Ni^{II} and Co^{II} were performed in a 1 cm cuvette with a 2 mL sample volume containing 0.5 μM Mag-Fura-2 and 1 mM $CaCl_2$ in a Chelex-treated 20 mM 3-(N-morpholino)propanesulfonic acid (MOPS, pH 7) buffer with 150 mM NaCl. The sample was allowed to equilibrate with stirring for 3 min after each addition of the competing metal stock before recording fluorescence excitation scans monitoring emission at 505 nm. Zn^{II} titrations were performed with 1 mM Ni^{II} (sulfate salt) as the competing ion in place of $CaCl_2$. Titration data (fluorescence excitation monitored at 330 nm) were fit to a 1-site binding model using Dynafit[48] assuming a Mag-Fura-2:Ca^{2+} K_d of 25 μM, which was found to be constant over a wide variety of pH and ionic strength conditions.[26] The resulting K_d values are listed in Table 1. The Mag-Fura-2:Zn^{II} K_d was back-calculated using the Mag-Fura-2:Ni^{II} K_d determined here.

^{BMOE}RIDC1$_2$:Mag-Fura-2 competition assays were performed in a 1 cm cuvette with a 1.5 mL sample volume containing 25 μM ^{BMOE}RIDC1$_2$ and 10 μM Mag-Fura-2 in Chelex-treated MOPS (pH 7) buffer with 150 mM NaCl. As with the titrations described above, samples were allowed to equilibrate under stirring for 3 min after the addition of each aliquot of the appropriate divalent metal stock before recording fluorescence excitation scans monitoring emission at 505 nm. Ni^{II} and Co^{II} binding to Mag-Fura-2 results in quenching of the florescence signal, which was subsequently followed using the emission readout using 372 nm excitation. Zn^{II} binding results in an increased fluorescence excitation at 323 nm, which was used as the excitation wavelength. All titration curves could be adequately described with a minimal (4 × 1) binding model consisting of four binding sites with equivalent half-saturation values listed in Table 1. Cu^{II} titrations were performed similarly to Ni^{II}, Co^{II}, and Zn^{II}, except Mag-Fura-2:Cu^{II} binding was monitored by the increase in absorbance at 300 nm, rather than by fluorescence.

Analytical Size Exclusion Chromatography (SEC). Size exclusion chromatography was performed on a Biologic DuoFlow FPLC system (Bio-Rad) equipped with a UV detector set to monitor absorbance at 280 nm. For each run, 100 μL of 25 μM ^{BMOE}RIDC1$_2$ in a 20 mM TRIS (pH 7) buffer with 50 mM NaCl and either 50 μM $ZnCl_2$ or 5 mM EDTA was injected into an analytical SEC column packed with Pall ACA54 resin (fractionation range = 5−70 kDa). The samples were eluted from the column at 0.5 mL/min in 20 mM TRIS (pH 7) with 50 mM NaCl, and additionally, 5 mM EDTA for the metal-free sample. The dead volume in Figure S5 (Supporting Information) is based on a ferritin (MW ∼ 500 kDa) standard run under conditions identical to the metal-free sample.

■ ASSOCIATED CONTENT

Supporting Information. Detailed views of RIDC1 interfaces, spectra for metal-binding assays, X-ray fluorescence spectra of the Zn^{II}−Cu^{II} cocrystal of ^{BMOE}RIDC1$_4$, size-exclusion chromatograms of ^{BMOE}RIDC1$_2$, and tables for X-ray data collection and refinement statistics. This material is available free of charge via the Internet at http://pubs.acs.org.

■ AUTHOR INFORMATION

Corresponding Author
*E-mail: tezcan@ucsd.edu.

■ ACKNOWLEDGMENT

This work was supported by the National Science Foundation (CHE-0908115), the Hellman Foundation, the Sloan Foundation, and the Arnold and Mabel Beckman Foundation. F.A.T. was in part supported by DOE Basic Energy Sciences, Biomolecular Materials Program (DE-FG02-10ER46677, crystallographic analyses). Portions of this research were carried out at SSRL, operated by Stanford University on behalf of the DOE.

■ REFERENCES

(1) Schmuck, C. *Angew. Chem., Int. Ed.* **2007**, *46*, 5830–5833.
(2) Ajami, D.; Rebek, J. *Proc. Natl. Acad. Sci. U.S.A.* **2007**, *104*, 16000.
(3) Gibb, C. L. D.; Gibb, B. C. *J. Am. Chem. Soc.* **2006**, *128*, 16498.
(4) Kramer, R.; Lehn, J. M.; Marquisrigault, A. *Proc. Natl. Acad. Sci. U. S. A.* **1993**, *90*, 5394.
(5) Caulder, D. L.; Raymond, K. N. *Acc. Chem. Res.* **1999**, *32*, 975.
(6) Klemm, J. D.; Schreiber, S. L.; Crabtree, G. R. *Ann. Rev. Immunol.* **1998**, *16*, 569.
(7) Mann, S. *Angew. Chem., Int. Ed.* **2008**, *47*, 5306–5320.
(8) Salgado, E. N.; Ambroggio, X. I.; Brodin, J. D.; Lewis, R. A.; Kuhlman, B.; Tezcan, F. A. *Proc. Natl. Acad. Sci. U.S.A.* **2010**, *107*, 1827.
(9) Salgado, E. N.; Radford, R. J.; Tezcan, F. A. *Acc. Chem. Res.* **2010**, *43*, 661.

(10) Bergdoll, M.; Eltis, L. D.; Cameron, A. D.; Dumas, P.; Bolin, J. T. *Protein Sci.* **1998**, *7*, 1661.
(11) Armstrong, R. N. *Biochemistry* **2000**, *39*, 13625.
(12) Volbeda, A.; Hol, W. G. J. *J. Mol. Biol.* **1989**, *206*, 531.
(13) Rausell, A.; Juan, D.; Pazos, F.; Valencia, A. *Proc. Natl. Acad. Sci. U.S.A.* **2010**, *107*, 1995.
(14) Rees, D. C.; Howard, J. B. *Curr. Opin. Chem. Biol.* **2000**, *4*, 559.
(15) Ali, M. H.; Imperiali, B. *Bioorg. Med. Chem.* **2005**, *13*, 5013.
(16) Thompson, M. C.; Busch, D. H. *J. Am. Chem. Soc.* **1964**, *86*, 3651.
(17) Creaser, I. I.; Geue, R. J.; Harrowfield, J. M.; Herlt, A. J.; Sargeson, A. M.; Snow, M. R.; Springborg, J. *J. Am. Chem. Soc.* **1982**, *104*, 6016.
(18) McMurry, T. J.; Raymond, K. N.; Smith, P. H. *Science* **1989**, *244*, 938.
(19) Dietrichbuchecker, C. O.; Sauvage, J. P.; Kern, J. M. *J. Am. Chem. Soc.* **1984**, *106*, 3043.
(20) Brodin, J. D.; Medina-Morales, A.; Ni, T.; Salgado, E. N.; Ambroggio, X. I.; Tezcan, F. A. *J. Am. Chem. Soc.* **2010**, *132*, 8610.
(21) Goodsell, D. S.; Olson, A. J. *Annu. Rev. Biophys. Struct.* **2000**, *29*, 105.
(22) Salgado, E. N.; Faraone-Mennella, J.; Tezcan, F. A. *J. Am. Chem. Soc.* **2007**, *129*, 13374.
(23) de la Torre, J. G.; Huertas, M. L.; Carrasco, B. *Biophys. J.* **2000**, *78*, 719.
(24) Raju, B.; Murphy, E.; Levy, L. A.; Hall, R. D.; London, R. E. *Am. J. Physiol.* **1989**, *256*, C540.
(25) Simons, T. J. B. *J. Biochem. Biophys. Methods* **1993**, *27*, 25.
(26) Golynskiy, M. V.; Gunderson, W. A.; Hendrich, M. P.; Cohen, S. M. *Biochemistry* **2006**, *45*, 15359.
(27) Krantz, B. A.; Sosnick, T. R. *Nat. Struct. Biol.* **2001**, *8*, 1042.
(28) Ghadiri, M. R.; Choi, C. *J. Am. Chem. Soc.* **1990**, *112*, 1630.
(29) Frausto da Silva, J. J. R.; Williams, R. J. P. *The Biological Chemistry of the Elements*; Oxford University Press: Oxford, U. K., 2001.
(30) Nolan, E. M.; Ryu, J. W.; Jaworski, J.; Feazell, R. P.; Sheng, M.; Lippard, S. J. *J. Am. Chem. Soc.* **2006**, *128*, 15517.
(31) Walkup, G. K.; Imperiali, B. *J. Am. Chem. Soc.* **1997**, *119*, 3443.
(32) Hunt, J. A.; Ahmed, M.; Fierke, C. A. *Biochemistry* **1999**, *38*, 9054.
(33) Waldron, K. J.; Robinson, N. J. *Nat. Rev. Microbiol.* **2009**, *7*, 25.
(34) Liu, J. B.; Dutta, S. J.; Stemmler, A. J.; Mitra, B. *Biochemistry* **2006**, *45*, 763.
(35) The initial concentration of the Zn_4:$^{BMOE}RIDC1_4$ sample applied to the SEC column is 25 μM (based on $^{BMOE}RIDC1_2$), at which no dimer would be expected to be present.
(36) On the basis of the available results, we cannot completely discount the possibility that the apparent Zn over Cu selectivity is due to the kinetic stability of Zn_4:$^{BMOE}RIDC1_4$ and that this species preferentially crystallizes out of a mixture of Zn and Cu adducts. Even if this were the case, our results on $^{BMOE}RIDC1_2$ represent a significant improvement of Zn^{II} selectivity over other divalent metal ions compared to the parent (pretemplated) species, MBPC1, which shows considerably higher affinities (as least 10-fold) for Cu^{II} and Ni^{II} over Zn^{II}: (a) Salgado, E. N. et al. *J. Am. Chem. Soc.* **2007**, *129*, 13374−13375. (b) Salgado, E. N.; et al. *Inorg. Chem.* **2009**, *48*, 2726–2728.
(37) Nelson, M. R.; Chazin, W. J. *Protein Sci.* **1998**, *7*, 270.
(38) Fritz, G.; Botelho, H. M.; Morozova-Roche, L. A.; Gomes, C. M. *FEBS J.* **2010**, *277*, 4578.
(39) Reyes-Caballero, H.; Campanello, G. C.; Giedroc, D. P. *Biophys. J.* **2011**, *156*, 103.
(40) Salgado, E. N.; Lewis, R. A.; Faraone-Mennella, J.; Tezcan, F. A. *J. Am. Chem. Soc.* **2008**, *130*, 6082.
(41) Salgado, E. N.; Lewis, R. A.; Mossin, S.; Rheingold, A. L.; Tezcan, F. A. *Inorg. Chem.* **2009**, *48*, 2726.
(42) Schuck, P. *Biophys. Chem.* **2004**, *108*, 187.
(43) Collaborative Computational Project, Number 4: *Acta Crystallogr.* **1994**, *D50*, 760−763.
(44) Vagin, A.; Teplyakov, A. *J. Appl. Crystallogr.* **1998**, *30*, 1022.
(45) Murshudov, G.; Vagin, A.; Dodson, E. *Acta Crystallogr.* **1996**, *D53*, 240.
(46) Emsley, P.; Cowtan, K. *Acta Crystallogr.* **2004**, *D60*, 2126.
(47) DeLano, W. L. *The PYMOL Molecular Graphics System*. http://www.pymol.org (accessed May 2011).
(48) Kuzmic, P. *Anal. Biochem.* **1996**, *237*, 260.